ELSEVIER

Polymer 42 (2001) 7701–7710

polymer

www.elsevier.nl/locate/polymer

Studies of non-solvent induced polymer coagulation by magnetic resonance imaging

P.R. Laity[a,*], P.M. Glover[b], A. Barry[c], J.N. Hay[a]

[a]*School of Metallurgy and Materials, University of Birmingham, Edgbaston, Birmingham B15 2TT, UK*
[b]*School of Physics and Astronomy, University of Nottingham, University Park, Nottingham NG7 2RD, UK*
[c]*School of Physics and Chemistry, University of Surrey, Guildford, Surrey GU2 5XH, UK*

Received 22 January 2001; received in revised form 28 February 2001; accepted 16 March 2001

Abstract

It is widely accepted that the morphology of a polymer membrane depends strongly on the conditions prevalent during coagulation. In particular, the composition changes which occur prior to coagulation and the subsequent phase change affect morphology and this, in turn, controls porosity, permeability and selectivity. For many applications, the optimal membrane structure combines a thin, dense layer for selectivity at high flux rates with a thicker, highly porous layer for mechanical strength. While there have been many studies into the development of membrane structures, these have largely relied on calculated composition changes using diffusion-based models

Magnetic resonance imaging has shown great benefit in studies of diffusion in polymers. In the present work, it has been used to follow composition and structural changes taking place during the coagulation of cellulose diacetate solution in acetone by immersion in water.

Keywords: Cellulose acetate; Coagulation; Magnetic resonance imaging

1. Introduction

It is well known that morphology plays an important part in controlling the selectivity and permeability of polymer membranes [1,2]. In general, more open, porous morphologies give greater permeability, but poorer selectivity, while denser morphologies result in higher selectivity but lower permeability. Higher permeability is also favoured by thinner membranes, but this has to be offset against their lower strength. A major advance in membrane science was the development of 'asymmetric' membranes combining a dense but very thin (i.e. less than 1 μm), selective layer over a much thicker, but highly porous support layer, by Loeb and Sourirajan [3].

It is also widely recognised that the morphology develops as a consequence of the phase separation processes during coagulation [4–6]. The onset of phase separation can be brought about by two distinct routes. Thermally-induced phase separation does not require mass transport, but the thermodynamic state of the polymer solution is altered by a change in temperature. In contrast, non-solvent induced phase separation occurs isothermally by mass transport and the exchange of solvent for non-solvent. This is usually achieved by 'wet-casting', in which the polymer solution is immersed in a bath of non-solvent. In the work presented here, an example of the immersion 'wet-casting' route has been studied.

The underlying theories of polymer coagulation have been reviewed by van de Witte et al. [5] and Wienk et al. [6]. The main points are demonstrated in Fig. 1, for a hypothetical non-solvent/solvent/polymer system. If the composition path remains within the homogeneous, single phase region of the diagram but moves towards higher polymer concentration (path A), 'vitrification' occurs as the viscosity increases and the solution reverts to a glass. This results in a dense polymer morphology, without porosity. This path is typical of the composition change during 'dry-casting' from a volatile solvent.

However, the composition path during dry-casting can be diverted if a less volatile non-solvent is also incorporated in the polymer solution. Under these conditions, a composition change more akin to wet-casting can be achieved.

By increasing the proportion of non-solvent (by wet-casting or dry-casting from mixed solution) the composition moves across the binodal into the miscibility gap or 'bi-phasic' region of the phase diagram (paths B, C or D). Phase separation results in a granular, porous morphology. Moreover, theory suggests several alternative phase separation

* Corresponding author.

0032-3861/01/$ - see front matter
PII: S0032-3861(01)00222-1

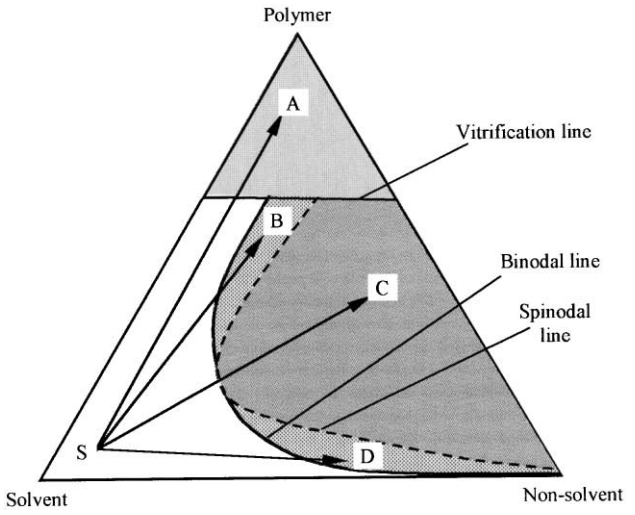

Fig. 1. Examples of composition pathways during coagulation. S: initial solution composition; A: vitrification and dense structure; B: nucleation and growth of polymer domains; C: spinodal decomposition into polymer domains and pores; D: nucleation and growth of non-solvent domains.

mechanisms. In the metastable regions between the binodal and spinodal curves (B and D), polymer-rich particles or liquid-filled pores form by 'nucleation and growth'. In contrast, in the unstable region bounded by the spinodal curve (path C), phase separation occurs by spontaneous growth of composition fluctuations. The process is further complicated when the polymer is crystallisable, since competition between liquid–solid and liquid–liquid separation processes can affect the morphology [7].

The coagulation of many different non-solvent/solvent/polymer combinations have been studied extensively [8–28]. However, while there are numerous publications describing the structures formed, few experimental results are available which follow the underlying composition changes. In most cases, discussions of the onset of phase separation and the observed polymer morphologies have been based on calculated composition changes derived from mathematical models of the solvent–non-solvent exchange. Elaborate and sophisticated diffusion models have been devised by McHugh and co-workers [11,20], Radovanovic et al. [16,17], Young and Chen [19], Reuvers and co-workers [21,22] and others [13,25,26,29]. However, in the absence of direct composition measurements, there

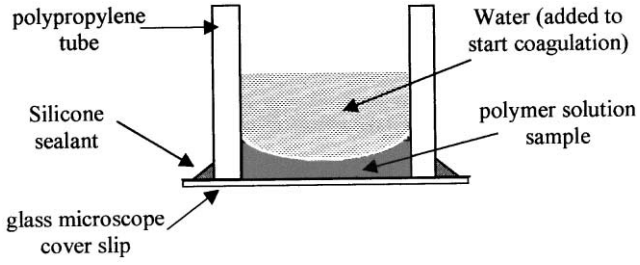

Fig. 2. Sample presentation for MRI experiments.

are two significant problems: (1) do these models adequately represent the physical processes occurring during non-solvent induced coagulation; (2) where components of the models are measured experimentally, are the values sufficiently accurate? In the present work, we demonstrate an experimental method which shows promise for following the composition and structural changes during coagulation.

Magnetic resonance imaging (MRI) is a powerful tool for studying both the distribution of liquids in porous or absorbent solids and movement due to flow or diffusion. The basic principles have been described by Callaghan [30] and Blumler et al. [31]. By applying a magnetic field gradient across the sample, the resonant frequency of the nuclei under observation (typically protons) encodes for position, while the characteristics of signal attenuation can be used to determine molecular mobility. Hence, MRI has been used extensively for studying the distribution and diffusion of water or other liquids in polymers and a wide range of porous materials [30–52]. Nevertheless, the potential of MRI for studying polymer coagulation appears to have been overlooked, hitherto.

The technique of Stray Field Imaging (STRAFI) is a variant of MRI which uses a high permanent magnetic gradient ($>10\ \mathrm{T\ m^{-1}}$) to image solid-like samples (i.e. having short relaxation times) in one dimension [53–55]. It is, therefore, particularly useful for observing thin planar homogeneous structures which change in one dimension only. Previously published studies included water diffusion in sandstone rock plugs [44], zeolite powder beds [56], fibrous cement tiles [57] and cellulose membranes [58], solvent diffusion in polymers [59] and the drying of paint films [60]. In the present work, STRAFI has been used to observe changes in composition, self-diffusion and relaxation times related to phase separation during coagulation of cellulose diacetate (CDA) from solution in acetone.

CDA was amongst the first polymers used to prepare synthetic membranes. Its solubility in a wide range of common solvents makes processing relatively easy and offers much scope for controlling the morphology by the choice of coagulation conditions. Loeb and Sourirajan used CDA to prepare integrally-skinned, asymmetric membranes [3] and CDA membranes are still widely used in water purification [1,2,61]. The development of morphology in membranes prepared from this polymer by non-solvent induced precipitation has consequently been the subject of much research [9,11,12,14,15,20–28].

2. Experimental

2.1. Sample preparation

A sample of cellulose diacetate (CDA, degree of substitution = 2.4) was dissolved in acetone (Aldrich, GPR grade) to give a solution of 27% by weight (in a closed

vessel to prevent evaporation of the solvent). A small portion (approximately 0.1 g) of the resulting solution was transferred to a sample holder, as shown in Fig. 2, covered (to minimise evaporation) and allowed to spread into a uniform layer approximately 500 μm thick. This was placed carefully into the spectrometer, such that any bubbles were avoided and the more even central part of the sample was above the detector coil assembly.

2.2. Magnetic resonance imaging

MRI measurements were performed on the permanent magnet STRAFI system at Surrey University [53–55]. This system employs a permanent magnet with shaped pole-pieces which produce a fixed planar homogeneous field gradient (G) of 17.53 T m^{-1} in the vertical direction. The excitation/detector coil assembly consisted of a solenoid with four turns of wire, 2 mm diameter, embedded in a resin block and covered with a layer of adhesive polyimide tape. The magnet was maintained at a temperature of 30°C to avoid frequency drift. The centre frequency of the spectrometer (Resonance Instruments, Witney, UK) was tuned to 29.7 MHz to bring the image of the sample into the centre of the field of view.

Magnetic resonance data were collected using a train of eight spin (plus stimulated) echoes ($N = 8$) from a pulse sequence defined as $90_x - \tau - [90_y - \tau - \text{echo} - \tau]_N - T_R$, where τ was the echo delay time. Each echo was sampled by acquiring 128 points (N_p) with a dwell time (t_{dwell}) of 1.6 μs. A relaxation delay (T_R) of 250 ms was used between scans and 256 scans were collected, giving a total scan time of 65 s. With the inclusion of a small amount of 'processing time', during which the data were saved onto the computer, the imaging process was repeated at intervals of 69 s. Each echo sample was Fourier-transformed to give the sample profile in the gradient direction. The intensity of the first (direct spin) echo image was multiplied by 1.5 to compensate for the additional contributions from other spin components in subsequent echoes [53]. The first four echoes were averaged to produce an image which was derived mainly from protons in moderately mobile solvent and H_2O within the polymer. Rapidly relaxing species with relatively short transverse relaxation times (T_2), such as solid polymer, and bulk liquids with relatively long spin–lattice relaxation times ($T_1 > 250$ ms) were not detected. However, a small contribution (less than 10% of the image strength) may have arisen from dissolved polymer, which is reported to have T_2 of a few milliseconds [62].

The pixel size was 6.54 μm, as given by:

$$r_{pix} = \frac{2\pi}{(G\gamma N_p t_{dwell})} \tag{1}$$

where γ was the magnetogyric ratio for protons (2.675×10^8 s^{-1} T^{-1}).

An image of the CDA solution sample was collected. Then a small amount of water (0.5 ml) was added by dropping pipette and further images collected until the signal strength had diminished to the level of background 'thermal' noise. The changing quantities of solvent and water present in the polymer gel were calculated by comparing corresponding images during coagulation of duplicate samples in D_2O and H_2O.

Self-diffusion coefficients (D) and transverse relaxation times were evaluated from the exponential decay rates of echo trains obtained at different echo delay times. For a train of echoes in a multi-echo sequence, the intensity decreased with time [$t = 2(n-1)\tau$, where n was the echo number] due to the effects of diffusion and T_2 relaxation [53], according to:

$$A_t = A_1 \exp\left\{\frac{-t}{T_2}\right\} \exp\left\{\frac{-\gamma^2 G^2 \tau^2 D t}{3}\right\} \tag{2}$$

Hence:

$$\ln\left\{\frac{A_t}{A_1}\right\} = -\left(\frac{1}{T_2} + \frac{\gamma^2 G^2 \tau^2 D}{3}\right) t \tag{3}$$

D and T_2 were evaluated from the slopes of straight line plots of $\ln\{A_t/A_1\}$ against t using simultaneous equations. The slope of the line (S_n), corresponding the echo delay time (τ_n), was given by:

$$S_n = -\left(\frac{1}{T_2} + \frac{\gamma^2 G^2 \tau_n^2 D}{3}\right) \tag{4}$$

Hence:

$$S_2 - S_1 = \left(\frac{\gamma^2 G^2 (\tau_1^2 - \tau_2^2) D}{3}\right) \tag{5}$$

$$D = \frac{3(S_2 - S_1)}{\gamma^2 G^2 (\tau_1^2 - \tau_2^2)} \tag{6}$$

Similarly:

$$T_2 = \frac{(\tau_1^2 - \tau_2^2)}{(S_1 \tau_2^2 - S_2 \tau_2^2)} \tag{7}$$

2.3. Electron microscopy

Cross-sections of the coagulated polymer samples were prepared by freeze-fracturing in liquid nitrogen. After drying under vacuum and coasting with gold, the cross-sections were viewed by scanning electron microscopy (SEM) at 20 kV and up to 5000 times magnification.

3. Results

The image through a sample of CDA solution in acetone, collected prior to starting coagulation, is shown in Fig. 3. Position is indicated in micrometres, as distance upwards from the glass cover-slip; the underside of the sample was set at zero and the upper surface was located at about

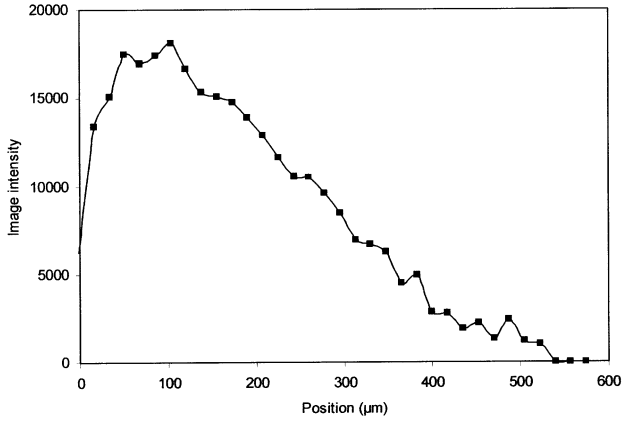

Fig. 3. Magnetic resonance image through a sample of CDA solution in acetone prior to the start of coagulation.

500–540 μm. The sloping upper edge of the image was attributed to a combination of two effects. The sample surface may have been uneven, due to the presence of ripples and a meniscus. More significantly, the signal from the upper surface was reduced, since it approached the limit of the field of view (FOV) of the GARField system. A key issue to be addressed in subsequent work will be sample presentation to overcome these problems. In the present work, however, to compensate for these effects, later images were normalised against the first profile during coagulation. This resulted in more uncertainty in the outer 150 μm of the image.

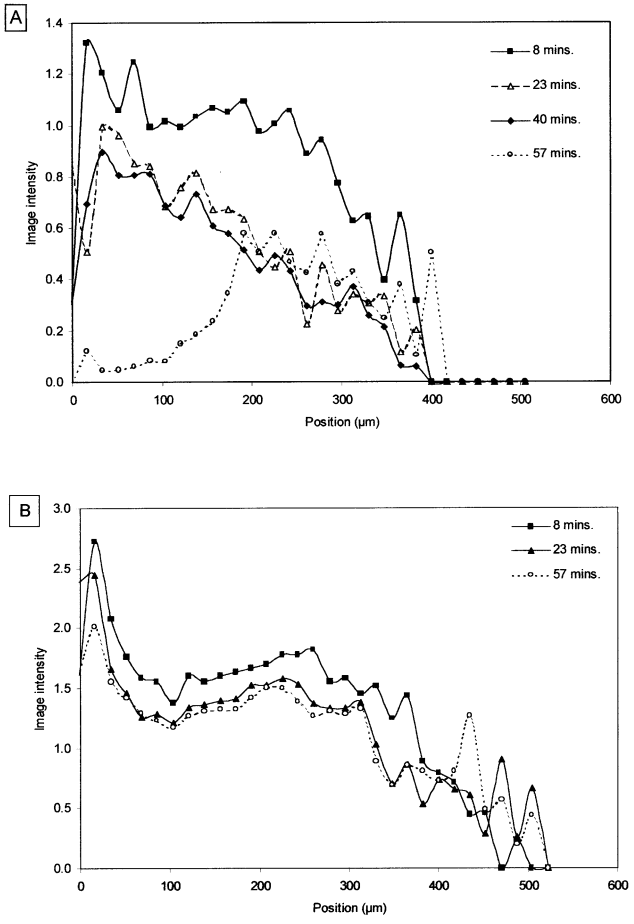

Fig. 4. Normalised images through CDA samples during coagulation: A: coagulation in D_2O; B: coagulation in H_2O.

3.1. MRI observations during coagulation

A series of images acquired during coagulation of CDA with D_2O and H_2O are compared in Fig. 4, demonstrating the composition changes within the polymer during coagulation. There appeared to be the distinct stages which occurred sequentially and at different depths below the CDA–water interface.

The first stage resulted in a rapid and progressive loss of the outermost part of the image during D_2O coagulation, consistent with acetone diffusing out of the sample. In contrast, the width of the images during the H_2O coagulation remained unchanged, but the intensities increased slightly. This was interpreted as an increase of water content throughout the entire CDA solution, with a complete displacement of acetone close to the CDA–water interface, causing a rapid precipitation of the polymer to form a 'skin'. It should be noted that pure water contains about 1.5 times as many hydrogen atoms as the same volume of pure acetone. This first stage appeared to be complete within about 8 min, by which time no image could be observed beyond 420 μm during the D_2O coagulation.

The widths of the images remained constant during the second stage of coagulation, but a gentle decrease in the signal strength was observed during the D_2O coagulation, while the images from the H_2O coagulation remained essentially constant. This was interpreted as a slow replacement of acetone by water within the sample, controlled by the 'skin' which had formed close to the CDA–water interface during the first stage of the coagulation.

During the third stage of the coagulation, the image from the D_2O coagulation decreased strongly within the lowest part of the sample, but remained fairly constant towards the middle. This may have been attributable to water leaking around the bottom of the sample, causing the CDA to float off the glass cover slip. A 'spike' in the MRI signal near the lower edge of the sample was observable from about 3 min into the H_2O coagulation, which may have been attributable to a thin layer of water between the CDA and the glass. However, while 'leakage' and coagulation from below cannot be ruled out, SEM studies revealed that large pores were formed within the lower part of the sample, which might also explain the changes observed in the images during this stage of coagulation. Many of these pores were sufficiently large for their contents to behave as 'bulk' liquid, with a relatively long spin–lattice relaxation time (T_1), as discussed by Glaves and Smith [63]. Hence, some acetone could effectively 'disappear', through a suppression

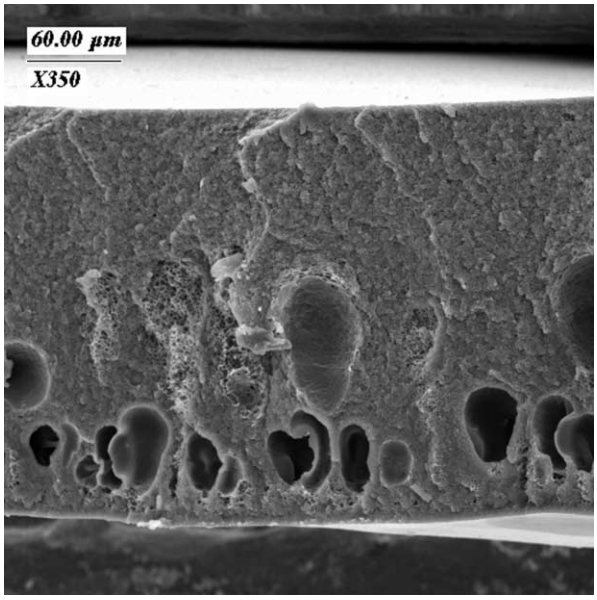

Fig. 5. SEM of cross-section of coagulated CDA, at 350× magnification, The lower surface of the cross-section was initially in contact with the cover slip during the MRI experiment.

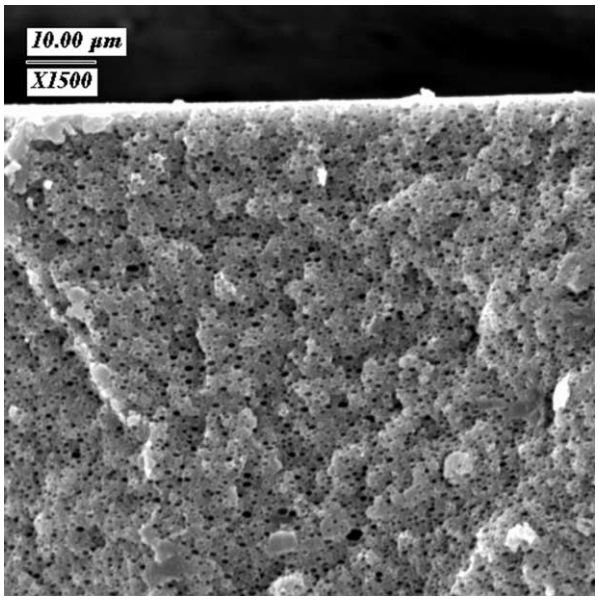

Fig. 6. SEM showing microporosity in upper region of coagulated CDA.

of its MRI signal, without actually moving away from the precipitated CDA.

3.2. Cross-section studies by SEM

The cross-section of a coagulated sample of CDA observed by SEM is shown in Fig. 5. It was found that the lower part of the sample, originally in contact with the cover slip, contained a considerable number of relatively large, elongated pores. These ranged from a few micrometres across to about 50 μm in length. Moreover, as Fig. 6 shows, even the denser upper region of the coagulated CDA contained a large number of 'micropores' of about 0.5–1 μm across and separated by apparently dense polymer. The lack of connectivity between these small pores suggests that they probably formed by nucleation and growth of a liquid phase, composed of water and acetone extracted from the CDA. (The alternative 'spinodal decomposition' mechanism is expected to produce mutually interconnected pores and polymer domains.)

SEM indicated the overall cross-section thickness of the precipitated CDA film to be about 250 μm, which was significantly smaller than indicated by MRI. Two possible explanations can be suggested for this. Firstly, as noted above, unevenness in the sample surface would cause some blurring of the MRI data, increasing the apparent sample thickness. Towards the edges of the samples, the surfaces curved upwards due to meniscus formation. However, the central areas, which were detected during the coagulation experiments, appeared reasonably uniform.

A second explanation is that sample shrinkage occurred after the end of the MRI experiments. The results from coagulation in D_2O suggested that a significant amount of acetone remained in the CDA. Shrinkage seems quite likely when this was removed by evaporation, as the samples were dried prior to gold-coating and SEM examination. Moreover, many of the small pores observable by SEM in Fig. 6 appeared slightly flattened, which would be consistent with a decrease in sample thickness. Shrinkage during casting CDA from acetone has also been observed previously by other authors: Stropnik et al. [9,12] reported from 75 to 88% decrease in thickness—albeit using a lower polymer concentration.

3.3. Composition changes during coagulation

Quantities of acetone and water at different levels within the CDA were estimated from the differences in images during the coagulation of identical samples of CDA/acetone solution in H_2O and D_2O. It was assumed that: (1) swelling or shrinkage of the CDA was not significant during the coagulation and (2) the strengths of MRI responses from protons in acetone and water within the CDA were similar. While these assumptions may not be entirely correct, they are believed to be adequate for the present purposes.

It should also be noted that the resulting compositions were averaged over the analysed regions of the polymer sample. These results did not depend on whether the samples were homogeneous or phase separated on a microscopic scale. However, phase separation on a coarser scale would cause suppression of the proton response if T_1 (the spin–lattice relaxation time) increased sufficiently. A significant loss of signal amplitude would occur if T_1 were of the order of T_R (the relaxation delay between scans) or longer.

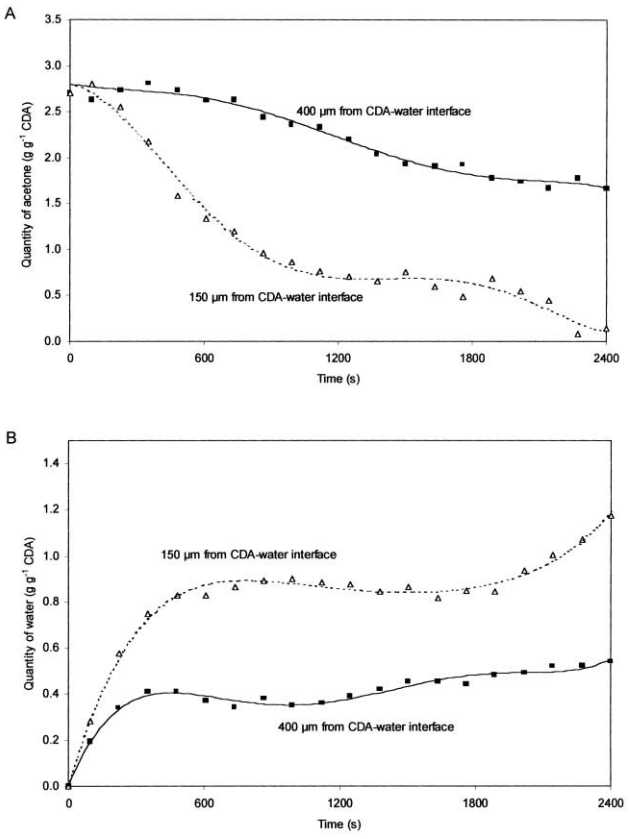

Fig. 7. Composition changes with time within CDA during coagulation in water: A, quantity of acetone in CDA; B, quantity of water in CDA.

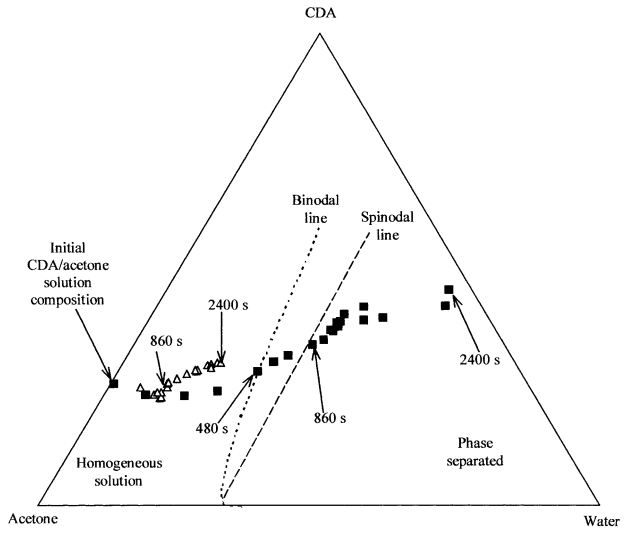

Fig. 8. Phase diagram and calculated average composition paths during coagulation; based on estimated composition changes during 40 min from start of coagulation; composition paths are shown for 150 μm (■) and 400 μm (△) from the CDA/water interface; times corresponding to various positions on each path are marked.

A complete replacement of acetone by water was evident at the CDA–water interface during the first minute of coagulation, consistent with the rapid formation of a polymer skin. However, this rate of composition change and the severely attenuated image near FOV limit prevented more detailed observations in the present experiments.

In contrast, it was possible to follow the more gradual composition changes that occurred deeper within the sample. The estimated weights of acetone and water associated with 1 g of CDA over the first 40 min of coagulation are shown in Fig. 7 for regions of the sample 150 and 400 μm below the water interface. It appeared that the initial influx of water slightly preceded the efflux of acetone, producing a slight dilution of the CDA during the early stages of coagulation. However, during the later stages, it was found that only approximately half as much water entered the CDA as acetone diffused out. This resulted in an increase in polymer concentration and may be consistent with the decrease in thickness, which was noted above.

The same data are presented as composition pathways through the phase diagram in Fig. 8. The binodal and spinodal lines are based on published work by Tsay and McHugh [20] and Reuvers et al. [21]. The composition paths were found to be curved, representing the initial dilution and subsequent increase in polymer concentration caused by the imbalance between acetone lost and water gained at different times during the coagulation. Although starting at different compositions, the shapes of these paths appeared quite similar to those calculated by Tsay and McHugh using a mathematical model [20]. (In fact, coagulation studies on 10% by weight CDA solution were attempted, to check the model described by Tsay and McHugh. However, these were unsuccessful as the coagulant mixed rapidly with the CDA solution, which expanded rapidly into a spongy mass.)

At 150 μm from the CDA–water interface, it appeared that the composition crossed the binodal line after 8 min and entered the unstable region enclosed by the spinodal after about 14 min. However, the estimated compositions were averaged over the regions of the samples analysed, irrespective of any phase separation on the micrometre scale. Phase separation could commence once the composition crossed the binodal. The position of the 'crossing point' on the binodal suggests that this would proceed by nucleation and growth of liquid droplets. SEM observations of small, isolated pores within the polymer were consistent with this process having taken place.

In contrast, the composition of the deepest parts of the sample remained within the homogeneous (solution) region of the phase diagram until considerably later in the coagulation. At 400 μm below the CDA–water interface, it appeared that the composition path had not reached the binodal after 40 min. This demonstrates that slow composition change within the interior of the coagulating sample could allow sufficient time for larger pores to grow.

3.4. Diffusion coefficient and T_2 measurements

Diffusion coefficients were evaluated for the CDA solution prior to coagulation from the changes in NMR echo intensity with time at different values of echo delay, using Eq. (6). It was assumed that the initial samples were homogeneous (i.e. no significant evaporation of solvent from the upper surface). Therefore, NMR data were averaged across the whole sample.

Plots in $\ln\{A_t/A_1\}$ versus time are shown in Fig. 9; the slopes were $-258 \pm 30\ s^{-1}$ and $-476 \pm 40\ s^{-1}$, for $\tau = 55$ and 200 μs, respectively, from which a value of $D = 0.8 \pm 0.2 \times 10^{-9}\ m^2\ s^{-1}$ was obtained, for the self-diffusion of acetone in 27% w/w CDA solution. This was about one fifth of the value given for pure acetone at 25°C by Tsay and McHugh [20] and Tasic et al. [64], demonstrating that the movement of solvent was impeded by the presence of the relatively immobile CDA molecules. This result was also roughly comparable to the diffusion coefficients reported by Ilyina and Daragan [62] for dimethyl sulphoxide and dimethylformamide solutions of cellulose acetates of various degrees of substitution.

A transverse relaxation time of $T_2 = 4.2 \pm 0.6$ ms was obtained from the data in Fig. 9. This is also consistent with acetone undergoing restricted motion, since the transfer of spin between nuclei becomes more efficient when molecular tumbling is slow [65].

A similar procedure was used to measure diffusion during coagulation in H_2O. No attempt was made to distinguish between acetone and water diffusion in the present experiments. Consequently, the diffusion coefficient obtained was a composite derived from the acetone and water present at any given time during coagulation.

Once coagulation had started, it was no longer valid to assume homogeneity across the entire cross-section. In principle, it should be possible to make spatially resolved diffusion measurements at various levels within the cross-section during coagulation. However, the signal was too weak from the upper part of the sample, which approached the FOV limit in the present experiments. This restricted measurements to the lowest 350 μm of the sample. In addition, there was too much uncertainty in the individual slope measurements, particularly at $\tau = 55$ μs, in the present experiment. Consequently, it was found to be necessary to use data which had been averaged over both position and time.

The change in diffusion coefficient, calculated from data averaged over the lowest 350 μm of the sample and five consecutive images during coagulation, is shown in Fig. 10. The diffusion became progressively slower, as coagulation proceeded. At the end of the experiment, a value of $D = 0.06 \pm 0.02 \times 10^{-9}\ m^2\ s^{-1}$ was obtained for (predominantly) water in CDA, which was considerably slower than the diffusion of acetone in the CDA solution at the start of coagulation.

This was also significantly slower than the diffusion of water in CDA membranes reported by Volkov et al. [66].

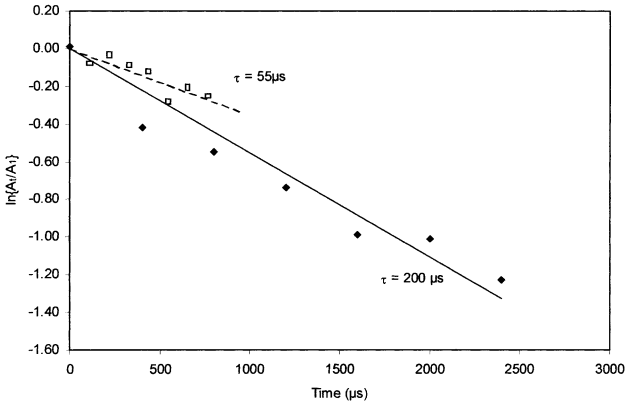

Fig. 9. Change of $\ln\{A_t/A_1\}$ with time, for CDA solution in acetone prior to coagulation.

Since the materials used were chemically similar, this implies that morphological differences between the samples affected the diffusion. It seems likely that there was negligible affinity between the CDA and water, which was contained predominantly within pores. Differences between the diffusion results can, therefore, be ascribed to differences in pore dimensions and connectivity.

During the same experiment, the transverse relaxation time was also evaluated from the averaged echo decay data. It appeared that T_2 initially increased to a maximum value of 20 ± 3 ms, at about 16 min into the coagulation; then it declined again, as shown in Fig. 11. At the end of the experiment T_2, for (predominantly) water in CDA was found to be 7 ± 1 ms. This behaviour may be due to the development of pores within the CDA. Initially, T_2 increased as pores grew in size and the liquid contained in the CDA became less affected by relaxation at polymer surfaces. However, as mobility increased within larger pores, this also affected the T_1 relaxation. It can be seen from Figs. 5 and 6 that the pore dimensions were distinctly bi-modal. Most of the pores were less than 1 μm across; but there were also a small number of relatively large pores with

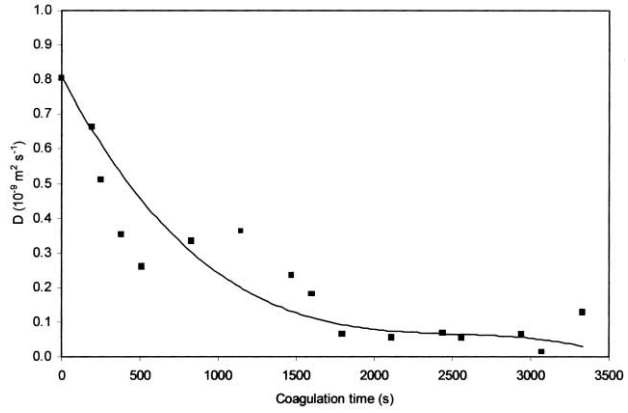

Fig. 10. Changes in diffusion coefficient with time during coagulation: from averaged echo decay data.

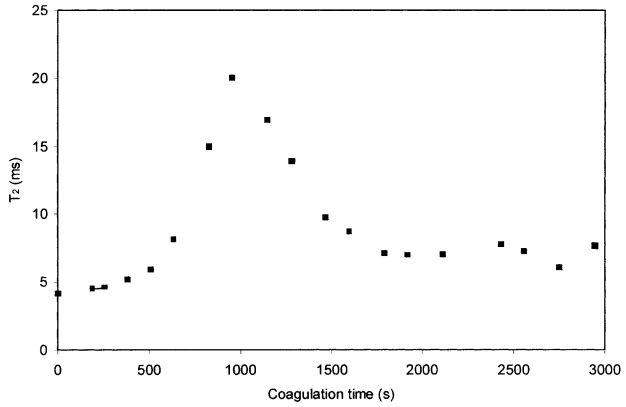

Fig. 11. Change in T_2 relaxation during coagulation; using averaged echo decay data.

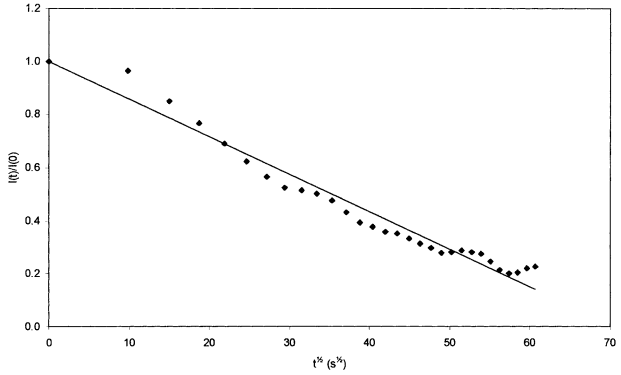

Fig. 12. Change in fraction of residual acetone in CDA with $t^{1/2}$.

diameters larger than 10 μm, within which any liquid would experience 'bulk-like' conditions, with T_1 relaxation time in excess of T_R. Consequently, the signal from the more mobile liquid was suppressed and only the constrained liquid within the smaller pores was detected.

For 'Fickian' systems, the diffusion coefficient can be obtained in various ways from the rate at which the diffusant is extracted out of the sample, as described by Crank [67]. It was assumed that the quantity of acetone in the CDA was proportional to the MRI signal during coagulation in D_2O; hence, it should be possible to estimate the diffusion coefficient from the rate of change of the integrated image. (Effectively, liquid contained within larger pores surrounded by polymer, but with longer T_1, was regarded as being 'outside'. This introduced a small over-estimation of the diffusion coefficient, since the presence of these pores decreased the diffusion distance 'out' of the polymer.)

A plot of the relative signal strength ($I(t)/I(0)$, where $I(t)$ was the total MRI signal from the acetone at time (t) against the square root of time ($t^{1/2}$) is shown in Fig. 12. The downward curvature near the start of the data may be attributed to acetone diffusing from the uppermost region of the sample, near the FOV limit, which could not be measured reliably. However, most of the plot was only slightly curved, demonstrating that the extraction of acetone from the coagulating CDA followed Fick's law reasonably closely. An effective diffusion coefficient is proposed, based on this overall change of composition, which disregards any diffusional changes within the sample itself. Assuming the extraction of acetone occurred only through one side of the sample (i.e. the other abutted the glass cover slip), the effective diffusion coefficient was obtained from the equation:

$$D = \frac{\pi d^2 S^2}{4} \tag{8}$$

where d is sample thickness and S is slope of the line. The data presented in Fig. 12 gave a slope of $-0.014 \pm 0.001\ s^{-1/2}$ from which $D_e = 0.04 \pm 0.01 \times 10^{-9}\ m^2\ s^{-1}$ was obtained.

Using a different procedure, the effective diffusion coefficient was also obtained from the slope of a plot of $\ln\{1 - I(t)/I(0)\}$ versus time, using the equation:

$$D = \frac{4Sd^2}{\pi^2} \tag{9}$$

The slope of the approximately linear portion of the graph shown in Fig. 13 was found to be $0.25 \pm 0.01 \times 10^{-9}\ m^2\ s^{-1}$ from which $D_e = 0.03 \pm 0.01 \times 10^{-9}\ m^2\ s^{-1}$ was obtained.

It is significant that these two methods of evaluating the effective diffusion coefficient were in reasonable agreement with each other, but the values obtained were an order of magnitude lower than that obtained from the echo attenuation during much of the coagulation. The most likely explanation is that the extraction of acetone out of the sample was controlled by a relatively impermeable skin of precipitated CDA. In fact, the estimation of D_e from the overall disappearance of the acetone signal agreed fairly well with the value obtained from the echo decay at the end of the coagulation, which represented water diffusion through the precipitated CDA. The skin also controlled the inward flux of water and, consequently, the rate of composition change leading to precipitation within the sample. Relatively fast diffusion was observed by the echo decay method in regions of the sample where the liquid state persisted. This hypothesis also explains the slight upward curvature in Fig. 12 and the downward curvature in Fig. 13, since the effective diffusion of acetone out of the CDA sample would be expected to slow down as the skin thickened.

4. Discussion

These relatively simple experiments demonstrate the potential for studying non-solvent induced polymer coagulation by MRI. Not only was it possible to follow composition changes by direct observations, but structural changes can also be inferred from measurements of diffusion coefficients and relaxation time constants.

From the present work it would appear that the coagulation of CDA from solution in acetone by immersion in water occurred in several distinct stages. Firstly, a rapid exchange

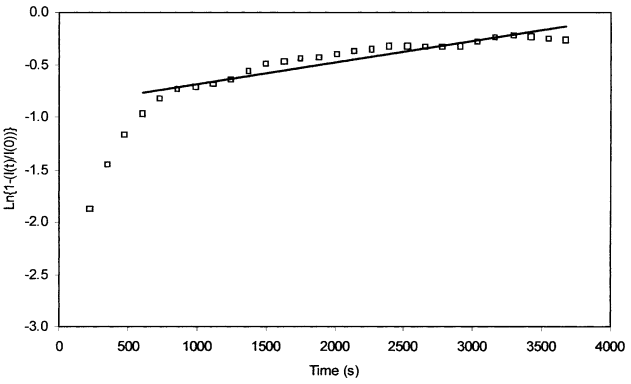

Fig. 13. Plot of $\ln\{1 - I(t)/I(0)\}$ against time for residual acetone in CDA.

of acetone and water took place at the surface of the polymer sample in contact with the coagulant and caused the polymer to precipitate.

The precipitated polymer was found to contain many small pores, which is consistent with phase separation occurring by nucleation and growth of liquid droplets within the CDA. The alternative, phase separation by spinodal decomposition, is expected to produce a mutually interconnected network of pores and polymer domains. However, this was not observable by SEM and seems inconsistent with the relatively low diffusion coefficient found for water within the precipitated CDA.

The phase separation resulted in a progressive removal of solvent from the polymer. Consequently, the polymer concentration between the pores increased until vitrification occurred. In this respect, it is probably significant that CDA is a random polymer, which cannot crystallise. It should also be noted that the paths indicated in Fig. 8 represented average compositions within analysed layers of the sample; whereas phase separation occurred at a scale which could not be resolved by MRI.

Although there were very many small water-filled pores in the polymer, they were isolated. The precipitated CDA was effectively impermeable to water. Hence, the initially precipitated polymer formed a 'skin' over the rest of the sample, which controlled subsequent diffusion into and out of the interior. MRI measurements demonstrated that the composition inside the sample changed more slowly after the polymer at the surface had precipitated. Also, echo decay indicated that faster diffusion occurred inside the sample compared with the extraction of acetone out of the sample. It appears that larger pores then formed as a result of the slower phase change deeper within the sample.

These measurements support the widely accepted mechanism for the coagulation of CDA from acetone solution into water, described by various authors [9,11,12,14,15,20–28]. The water/acetone/CDA system is well characterised and values for the physical parameters required to construct diffusion-based models of coagulation have been published. However, the methods we have demonstrated in this work can also be applied to more obscure systems, for which models are less readily available. For example, the diffusion coefficients used in the Tsay and McHugh model [14,20] depended on composition, but not on the time since phase separation started. Yet, time-dependence could be an important aspect of systems in which the polymer precipitates by a spinodal decomposition mechanism, such that the diffusion coefficients depend on the magnitude as well as scale of the composition fluctuations.

5. Conclusions

MRI is a very powerful method for studying non-solvent induced polymer coagulation, giving information on composition and morphology. The results of the present study were in agreement with the mechanism of CDA coagulation proposed by others [9,11,12,14,15,20–28].

This appears to be the first such application of MRI. However, it seems likely that similar experimental results could be obtained from a other non-solvent/solvent/polymer systems, including those for which models are less readily available.

References

[1] Baker RW. Membrane technology. In: Kroschwitz JI, Howe-Grant M, editors. Kirk-Othmer encyclopedia of chemical technology, 4th ed. New York: John Wiley and Sons, 1994. p. 135–93.
[2] Mulder M. Basic principles of membrane technology. Dordrecht, The Netherlands: Kluwer Academic, 1992.
[3] Loeb S, Sourirajan S. Advances in Chemistry Ser. 28, Saline Water Conversion—II (American Chemical Society, Washington, 1963), 117, Sea water demineralisation by means of an osmotic membrane.
[4] Kesting RE. J Appl Poly Sci 1990;41:2739.
[5] Van de Witte P, Dijkstra PJ, van den Berg JWA, Feijen. J Memb Sci 1996;117:1–31.
[6] Wienk IM, Boom RM, Beerlage MAM, Bulte AMW, Smolders CA, Strathmann H. J Memb Sci 1996;113:361–71.
[7] Cheng L-P, Young T-H, Chuang W-Y, Chen L-Y, Chen L-W. Polymer 2001;42:443–51.
[8] Chuang W-Y, Young T-H, Chui W-Y, Lin C-Y. Polymer 2000;41:5633–41.
[9] Stropnik C, Musil V, Brumen M. Polymer 2000;41:9227–37.
[10] Won J, Kang YS, Park HC, Kim UY. J Memb Sc. 1998;145:45–52.
[11] Barton BF, Reeve JL, McHugh AJ. J Poly Sci: part B: Poly Phys 1997;35:569.
[12] Stropnik C, Germic L, Zerjal B. J Appl Poly Sci 1996;61:1821.
[13] Young T-H, Chen L-W. Desalination 1995;103:233.
[14] McHugh AJ, Tsay CS. J Appl Poly Sci 1992;46:2011.
[15] Gaides GE, McHugh. J Memb Sci 1992;74:83.
[16] Rodovanovic P, Thiel SW, Hwang S-T. J Memb Sci 1992;65:231–46.
[17] Radovanovic P, Thiel SW, Hwang S-T. J Memb Sci 1992;65:213–29.
[18] Kang YS, Kim HJ, Kim UY. J Memb Sci 1991;60:219–32.
[19] Young T-H, Chen L-W. J Memb Sci 1991;59:169–81.
[20] Tsay CS, McHugh AJ. J Poly Sci: part B: Poly Phys 1990;28:1327–65.
[21] Reuvers AJ, Smolders CA. J Memb Sci 1987;34:67–86.
[22] Reuvers AJ, van den Berg JWA, Smolders CA. J Memb Sci 1987;34:45–65.
[23] Reuvers AJ, Altena FW, Smolders CA. J Poly Sci: part B: Poly Phys 1986;24:793–804.

[24] Mulder MHV, Oude Hendrikman J, Wijmans JG, Smolders CA. J Appl Poly Sci 1985;30:2805–20.
[25] Neogi P. J AIChE 1983;29:402–10.
[26] Cohen C, Tanny GB, Prager S. J Poly Sci Poly Phys Edn 1979; 17:477–89.
[27] Panar M, Hoehn HH, Hebert RR. Macromolecules 6;1973:777–80.
[28] Strathmann H, Scheible P, Baker RW. J Appl Poly Sci 1971;15:811–28.
[29] Termonia Y. J Poly Sci: part B: Poly Phys 1995;33:279.
[30] Callaghan PT. Principles of magnetic resonance microscopy. Oxford: Clarendon Press, 1991.
[31] Blumler B, Blumich P, Botto RE, Fukushima E, editors. Spatially resolved magnetic resonance. Weinheim; Wiley-VCH, 1998.
[32] Harding SG, Gladden LF. Mag Res Imag 1998;16:647–9.
[33] Stapley AGF, Fryer PJ, Gladen LF. AIChE J 1998;44:1777–89.
[34] Kojima M, Ando S, Kataoka K, Hirota T, Aoyagi K, Nakagami H. Chem Pharm Bull 1998;46:324–8.
[35] Hyde TM, Gladden LF. Polymer 1998;39:811–9.
[36] Harding SJ, Johns ML, Pugh SR, Fryer PJ, Gladden LF. Food Add Contam 1997;14:583–9.
[37] Stapley AGF, Hyde TM, Gladden LF, Fryer PJ, Int J. Food Sci Technol 1997;32:355–75.
[38] Lane DM, McDonald P. J. Polymer 1997;38:2329–35.
[39] Halse MR. Mag Res Imag 1996;14:745–50.
[40] McDonald PJ. Mag Res Imag 1996;14:807–10.
[41] Ercken M, Adraiensens P, Reggers G, Carleer R, Vanderzande D, Gelan J. Macromols 1996;29:5671–7.
[42] Hyde TM, Gladden LM, Mackley MR, Gao P. J Poly Sci: part A: Poly Chem 1995;33:1795–806.
[43] Stapley AGF, Sousa-Goncalves JA, Hollewand MP, Gladden LF, Fryer P. Int J Food Sci Technol. 1995;30:639–54.
[44] Roberts SP, McDonald PJ, Pritchard T. J Mag Res series A 1995;116:189–95.
[45] Halse MR, Rahman HJ, Strange JH, Physica B. 203 1994:169–85.
[46] Perry KL, McDonald PJ, Randall EW, Zick K. Polymer 1994;35: 2744–8.
[47] Webb AG, Motsegood K, Clarkson RB. Fuel 1993;72:1235–7.
[48] Jezzard P, Wiggins CJ, Carpenter TA, Hall LD, Barnes JA, Jackson P, Clayden NJ. J Mat Sci 1992;27:6365–70.
[49] Jezzard P, Wiggins CJ, Carpenter TA, Hall JA, Jackson P, Clayden NJ, Walton NJ. Adv Mat 1992;4:82–90.
[50] Webb AG, Hall LD. Polymer 1991;32:2926–38.
[51] Webb AG, Hall LD. Polym Comm 1990;31:422–5.
[52] Webb AG, Hall LD. Polym Comm 1990;31:425–7.
[53] McDonald PJ. Prog. Nucl Mag Res Spec 1997;30:69–99.
[54] McDonald PJ. Spectroscopy Europe 1995;7:25–30.
[55] Glover PM, McDonald PJ, Newling B. J Mag Res 1997;126:207.
[56] Hughes PDM, McDonald PJ, Smith EG. J Mag Res Series A 1996;121:147–53.
[57] Bohris AJ, Newling B, McDonald PJ, Raoof A, Tran NL. J Mat Sci 1998;33:859.
[58] Laity PR, Glover PM, Godward J, McDonald PJ, Hay JN. Cellulose 2000;7:227–46.
[59] Lane DM, McDonald PJ. Polymer 1997;38:2329.
[60] Glover PM, Aptaker PS, Bowler JR, McDonald P, Ciampi EJ. J Mag Res 1999;139:90.
[61] Ho WSW, Sirkar KK, editors. Membrane handbook. New York: Van Nostrand Reinhold, 1992.
[62] Ilyina E, Daragan V. Macromolecules 27;1994:3759–63.
[63] Glaves CL, Smith DM. J Memb Sci 1989;46:167–84.
[64] Tasic AZ, Djordjevic BD, Servanovic SP, Grozdanic DK. J Chem Eng Data 1981;26:118–20.
[65] Sanders JKM, Hunter BK. Modern NMR spectroscopy, a guide for chemists. Oxford: Oxford University Press, 1993.
[66] Volkov VI, Korotchkova SA, Nesterov IA, Oha H, Guo Q, Huang J, Chen. J Memb Sci 1996;110:1–11.
[67] Crank J. The mathematics of diffusion. 2nd ed. Oxford: Clarendon Press, 1975.